



HAL
open science

Integration of digital imagery for topology optimization

Zoubir Atmani, Alexis Iung, Jean-Pierre Radoux, Nadhir Lebaal

► **To cite this version:**

Zoubir Atmani, Alexis Iung, Jean-Pierre Radoux, Nadhir Lebaal. Integration of digital imagery for topology optimization. *International Journal for Simulation and Multidisciplinary Design Optimization*, 2023, 14, pp.4. 10.1051/smdo/2023004 . hal-04142386

HAL Id: hal-04142386

<https://hal.science/hal-04142386>

Submitted on 26 Jun 2023

HAL is a multi-disciplinary open access archive for the deposit and dissemination of scientific research documents, whether they are published or not. The documents may come from teaching and research institutions in France or abroad, or from public or private research centers.

L'archive ouverte pluridisciplinaire **HAL**, est destinée au dépôt et à la diffusion de documents scientifiques de niveau recherche, publiés ou non, émanant des établissements d'enseignement et de recherche français ou étrangers, des laboratoires publics ou privés.

Integration of digital imagery for topology optimization

Zoubir Atmani¹, Alexis Iung¹, Jean-Pierre Radoux¹, and Nadhir Lebaal^{2,*} 

¹ MOBHEEL, Département de recherche de Capgemini Engineering, 90400 Meroux-Moval, France

² ICB UMR 6303 CNRS, Univ. Bourgogne Franche-Comté, UTBM, Belfort, France

Received: 20 October 2022 / Accepted: 30 March 2023

Abstract. To manufacture high-quality products with low manufacturing costs and optimal performance, better design concepts are required. The initial design concept can lead to inefficient structural design and higher manufacturing costs if the topology is not optimal. Topology optimization enables designers to reach their design goals faster, more accurately, and cost-effectively. However, the geometry obtained through topology optimization is not manufacturing-ready due to non-smooth boundaries and gray level images, which require post-processing design implementation by engineers. Various researchers have used different image processing techniques to convert the gray image into a binary map to address this issue. This paper focuses on using image processing to evaluate the differences in optimal designs induced by meshing. This study aims to aid in the parametric understanding of different designs targeting the same application by introducing two new parameters: similarity ratio and conformity ratio. The results compare an optimal geometry obtained using structured and unstructured meshes. Topological optimization algorithms applied to mechanical problems allow for reducing a structure's mass while ensuring its rigidity. However, the final structures may differ for the same problem depending on whether they were meshed regularly or irregularly. This article characterizes the differences between the two final structures using an image processing approach.

Keywords: 2D topological optimization / regular mesh / irregular mesh / image treatment for mechanical application

1 Introduction

Due to the complexity of its calculations, topological optimization and meshes are closely linked. Most of the studies reported in the literature have been carried out using a regular mesh on simple mechanical problems such as embedded beams and double-supported beams [1,2]. Although the number of elements strongly influences the final design of the optimized structure, and the complexity of the structure evolves with it, very few studies deal with the influence of this parameter. Sigmund et al. [2] discuss this in their paper but leave the question open: “should the refinement of the mesh model the same optimal structure with a better description of the boundary conditions and not give a different structure with more detail and quality?”

To our knowledge, there is very little research dealing with topological optimization from an irregular mesh, even though this type of mesh is better suited to complex geometries. Thore et al. [3] conducted a study to compare the results of topological optimization of a regularly and

irregularly meshed double-supported beam. The primary goal of the paper was to evaluate the influence of the penalty factor on additive fabrication stresses. However, the authors conducted this study without any penalty filter and thus obtained topological optimization results from the two meshes discussed previously. Despite some local dissimilarities, the two structures presented fairly similar designs.

Therefore, the present article aims to explore whether there is a fixed topological optimization profile obtained after convergence of compliance.

2 Principle

2.1 Positioning the problem

The study was conducted on a 20×10 mm beam, fixed at one end and subjected to a 100 N force at the other end. The dimensions were chosen to satisfy the small disturbance hypothesis. The material parameters considered are: $E = 200$ GPa and $\nu = 0.3$.

The topological optimization was carried out using the in-house developed ELiOT software [4], which allows calculations from a model created by FreeCAD finite

* e-mail: Nadhir.lebaal@utbm.fr

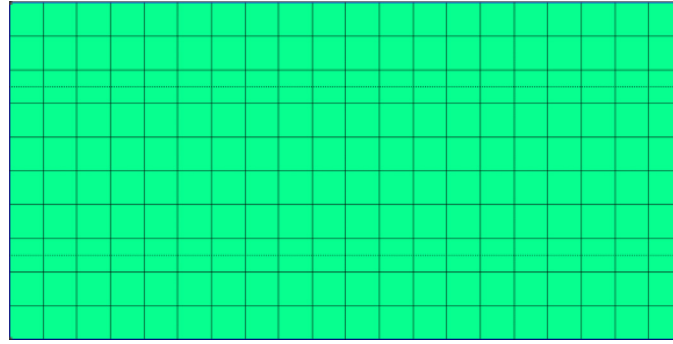


Fig. 1. Regular mesh with an internodal distance of 1 mm.

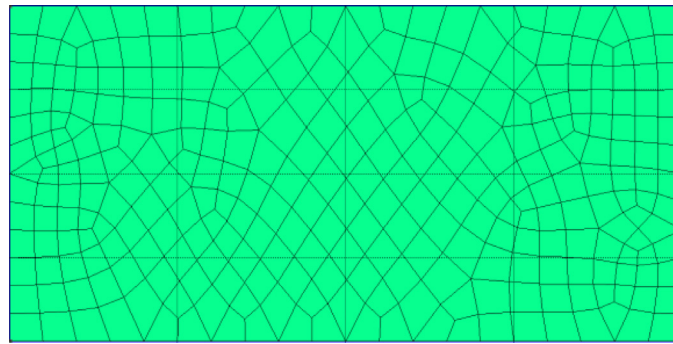


Fig. 2. Irregular mesh with an internodal distance of 1 mm.

element calculation codes and meshed with GMSH [5,6]. The constraint applied to the ELiOT code consisted of halving the mass of the initial object (volume fraction, $f_v = 0.5$), and the optimization algorithm used was the OC (optimal criteria) method.

The beam was meshed in two different ways: regularly (Fig. 1) and irregularly (Fig. 2) with quadrangular elements. As the number of elements was not the same for both meshes, the inter-node distance was considered as the parameter to be varied (Tab. 1).

The coordinate table contains the coordinates of each node in the mesh. It is represented by a matrix that has as many columns as the number of dimensions in the problem and as many rows as the number of nodes in the mesh. The connectivity table is used to define the connections between the nodes in the mesh. The number of rows in the table corresponds to the number of elements in the mesh, and the number of columns corresponds to the number of edges in the element being considered.

A mesh is considered regular (Fig. 1) when all its edges have the same connectivity. It is created by replicating an elementary mesh shape multiple times, and each element can be defined from another one.

A mesh is said to be irregular when its elements are arranged in a disorderly manner (Fig. 2). As the numbering of nodes and elements is often random, only the coordinate and connectivity tables can be used to navigate this type of mesh [7].

Given these considerations, it is challenging to make a direct comparison between these two meshes. To address this issue, a comparison by image processing has been proposed.

Table 1. Size and number of elements according to the type of mesh.

Internodal distance (mm)	Number of elements in the regular mesh	Number of elements in the irregular mesh
0.08	31250	39424
0.1	20000	24688
0.2	5000	6246
0.25	3200	3950
0.5	800	1024
1	200	298

2.2 Mechanics and image treatment

In the literature, image processing is predominantly utilized in mechanical problems with experimental settings, to measure the displacement of a point during manipulation. For this, a speckle is applied to the studied piece and photographs are taken at different instances during the test. Image correlation software is then utilized to track the path followed by the point of interest, to determine its displacement and subsequently, its deformation field Chu et al. [8]. A less significant, yet equally interesting objective for industry, is to determine the spatial distribution of the material parameters characterizing the studied sample Belis et al. [9]. Image correlation also allows for tracing the history of a crack and identifying its origin [10,11].

To establish a connection between image processing and digital simulation, it is essential to define a mathematical model before conducting this study. As the optimized beam has intermediate densities specific to the OC method, it is considered heterogeneous. Thus, it is possible to construct a Representative Elementary Volume (REV) to homogenize the heterogeneities. This requires defining different scales, each with a characteristic size, including one for the structure, one for the pixel, and one for the element. The pixel serves as the REV and its size influences the accuracy of the final results. In brief, this method involves drawing a regular grid, with a tile size that adheres to certain conditions, on the optimized structures obtained. This step allows for the regularization of any mesh, and each tile becomes a pixel in the final image with a single value.

In the case of the OC method, the topological optimisation algorithm follows the following objective function:

$$\begin{cases} \min_{\rho} : c(\rho) = U_e T \cdot K_e \cdot U_e \\ \text{subject to: } \{V(\rho) \\ V_0 = f_v K \cdot U = F_{10} - 3 < \rho < 1\} \end{cases} \quad (1)$$

Where:

- c is the compliance
- U_e is the displacement of the considered element.
- V is the volume of the optimized structure.
- V_0 is the initial volume of the structure.
- ρ is the intermediate density.

For the following, two writing will be used:

- N_p is the number of pixels of the image.
- N_e is the number of elements of the structure.

The volume of the structure after optimisation is, by definition:

$$V(\rho) = \frac{V_0}{N_e} \sum_1^{N_e} \rho_e. \quad (2)$$

with ρ_e the intermediate density of the considered element.

To link the three scales presented above, the homogenisation method will be used here. It consists in averaging the effects of heterogeneities within a REV in order to determine the macroscopic effects of the studied structure. To be able to apply this method, the following two conditions must be respected:

- The pixel size must be very small in front of that of the structure in order for the structure to be considered as a continuous environment, thus $N_p \gg 1$.
- The pixel size must be very large in front of the element size in order to neglect the fluctuation in behaviour between a point and its neighbour. The material is then considered to be macroscopically homogeneous. Thus, it is necessary that $N_e \gg N_p$.

The intermediate density of a pixel is then equal to the average of the intermediate densities of the elements contained in that pixel:

$$\rho_p = \frac{N_p}{N_e} \sum_1^{N_e/N_p} \rho_e. \quad (3)$$

Depending on the intermediate pixel density, the volume of the structure after optimisation is therefore:

$$V(\rho) = \frac{V_0}{N_p} \sum_1^{N_p} \rho_p. \quad (4)$$

Finally:

$$V(\rho) = \frac{V_0}{N_e} \sum_1^{N_p} \sum_1^{N_e/N_p} \rho_e. \quad (5)$$

Remark:

In practice, it is the contrast of the C_p (between 0 and 255) that will be measured, so the intermediate density of a pixel is:

$$\rho_p = \frac{C_p}{255}. \quad (6)$$

2.3 Image creation from the optimized structure

The files generated by the topological optimization code contain the element number and the assigned intermediate density. Using equation (6), these intermediate densities can be converted into contrasts. In both mesh cases, the files are sorted in ascending order based on the elements, and the images are constructed in rows. However, for the irregular mesh, the first element of the mesh may not correspond to the first pixel of the image, and therefore, the elements need to be ordered to obtain an accurate image. An algorithm is used to calculate the center of gravity of each element and sort them in ascending order of rows and columns.

One of the main assumptions of this study is that the number of elements in the structure is much greater than the number of pixels in the image. Therefore, it is necessary to average the intermediate densities of the elements within a pixel using equation (3). This step is accomplished by a pooling operation, which is commonly used in convolutional neural network algorithms Sosnovik et al. [12]. This operation groups elements together and creates a sub-sampled image.

2.4 Calculation of the image dissimilarity

Each pixel of a grayscale image has a value between 0 and 255 and corresponds to the average of the intermediate densities of the elements contained in that pixel. Let's consider two images resulting from topological optimisation. One obtained from a regular mesh I_{reg} and the other from an irregular mesh I_{irreg} . The dissimilarity between two images is defined by Ardeshir et al. [13]:

$$D = \sum_{i=1}^n |I_{reg,i} - I_{irreg,i}|. \quad (7)$$

It has to be noted that equation (7) is a variation of the Manhattan distance.

Remark 1:

For further calculations, equation (7) will be used. However, for visual results, equation (7) will become:

$$D_{inv} = 255 - D \quad (8)$$

The value 255 in this formula will invert the contrast so that the result is more visual (black on white instead of white on black). When subtracting, the algorithm will remove the identical material between the two images, symbolised by white in the final image, and will finally display only the excess material.

Remark 2:

In order for the calculation to be carried out, the images must have the same dimensions.

Considering (6), equation (7) becomes:

$$D = 255 \times \sum_{i=1}^n |\rho_{reg,i} - \rho_{irreg,i}|. \quad (9)$$

However, if only one image is taken into account, the equation becomes:

$$D_1 = 255 \times \sum_{i=1}^n |\rho_{reg,i}| = V_{final} \quad (10)$$

For an image, the dissimilarity corresponds to the final volume of the structure after optimisation. Thus, the measurement of dissimilarities between two images corresponds to the difference in final volume between the two optimised structures. The equation thus becomes:

$$D = 255 \times \sum_{i=1}^n |\rho_{reg,i} - \rho_{irreg,i}| = \Delta V_{final}. \quad (11)$$

Given the definition of the volume fraction in equation (1) and equation (11), it will be possible to retrieve the volume fraction (Eq. (12)) and the difference in volume fraction (Eq. (13)) between two structures via an image processing method:

$$f_v = \frac{V_{final}}{V_{initial}} = \frac{D_1}{V_{initial}}, \quad (12)$$

and:

$$\Delta f_v = \frac{D}{V_{initial}}. \quad (13)$$

Two coefficients will be defined for the continuation of the:

- The compliance ratio, which ideally should be 1. This calculation can be done on each image to be studied and will determine whether the image of the optimised structure complies with the desired final volume. It is defined by :

$$\tau_c = \frac{D_1}{V_{f,th}}. \quad (14)$$

The dissimilarity rate, which ideally should be 0. This calculation can only be performed to compare two images and will determine whether the two images are similar. It is defined by:

$$\tau_d = \frac{D}{V_{f,th}}. \quad (15)$$

In these two expressions (Eqs. (14) and (15)), $V_{f,th}$ corresponds to the theoretical final volume of the optimised structure, i.e. the one imposed by the user at the beginning of the topological optimisation code.

It should be noted that the results of equations (10) and (11) will be a number of pixels and not a volume as conventionally defined.

An important remark is also to be taken into consideration for the compliance rate and the dissimilarity rate: these are coefficients defined in a global way. This means that they perform calculations on the entire image without determining where the differences will be most marked.

3 Results

3.1 Study of mechanical properties

The parameter that takes into account mechanical properties in the available topological optimization code is compliance. This parameter will be examined by varying the characteristic length of the different meshes (Fig. 3). Other parameters, such as volume fraction, could have been considered. However, the quality of the result will be influenced more by the accuracy of the machine used for the calculations rather than the mesh size.

Figure 3 clearly shows that the smaller the size of the element, i.e. the more elements in the mesh, the lower the compliance. A convergence step can be observed from an element size of 0.25 mm upwards.

Note that the relative deviation between the compliance values obtained from a regular mesh and an irregular mesh is less than 2% for an element size of 0.5 mm, and finally decreases to 0.3% for an element size of 0.08 mm. Thus, the mechanical properties after topological optimization of a regularly or irregularly meshed structure are similar. The two meshes are therefore equivalent.

3.2 Influence of the REV size on the volume fraction

In the mechanics and image processing section, it was observed that the Representative Elementary Volume (REV) is equivalent to a pixel and represents the average of intermediate densities of the elements composing that pixel. A study was conducted on the number and shape of elements that constitute the REV. The regular structure with 80,000 elements was used for comparison. Various

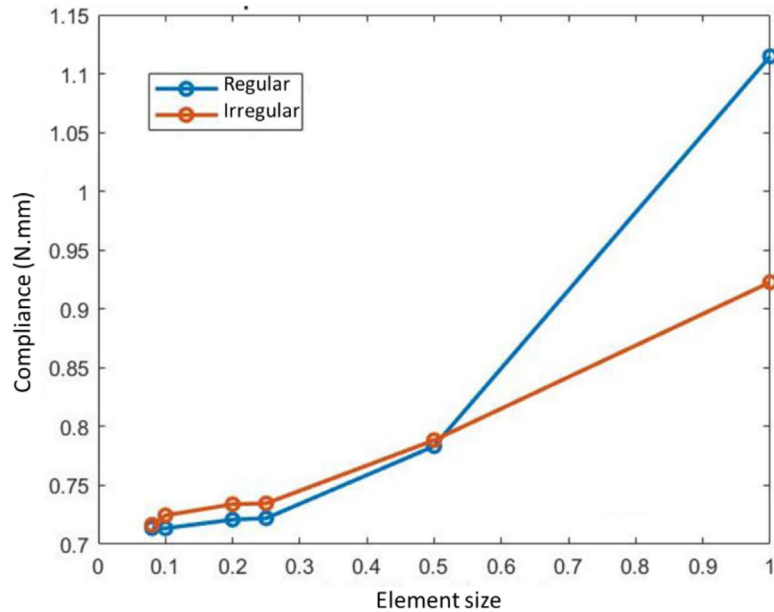


Fig. 3. Compliance vs element size for a regular mesh (in blue) and irregular mesh (in red).

sizes and shapes of REV were applied to this structure to determine their potential effects on the structure's volume fraction. The results are summarized in Table 2, which includes the facies of the images obtained after applying the REV to the initial image (measuring 200×400), the size of the REV, the size of the final image, and the number of elements per REV.

3.3 Study of dissimilarity between regular and irregular meshes

For this study, the code allowing the elements to be arranged in a certain order is only functional for the regular mesh. For irregular meshing, since the number of elements per column is not fixed according to the number of rows, it is difficult to construct an image from this data. The images required for this study were therefore cut directly from Paraview using the capture tool.

The results are summarised in Table 3. It contains the facies of regular and irregular structures, the volume fraction calculated with the image processing code, the compliance rate and the dissimilarity rate.

4 Discussion

4.1 Influence of REV size on the volume fraction

Figure 4 shows the influence of the size of the REV on the volume fraction. First of all, it is useful to point out that, despite a fairly marked distribution of points, the results remain close to the imposed volume fraction, i.e. 0.5. Thus, for Figure 4, the results, although close to reality, seem to depend on the number of elements that make up the REV: between 2 and 32 elements per REV, the volume fraction does not vary greatly. However, from 64 elements per REV, the volume fraction increases; this means that

the differences in intermediate densities between the elements become too great not to influence the quality of the REV.

Some REV have the same number of elements but not the same volume fraction. Figures 5 and 6 are intended to determine the influence of the REV dimensions on the quality of the volume fraction.

Concerning Figure 5, the number of lines in the REV does not appear to have a significant impact because a convergence of the volume fraction can be observed for 1 and 2 lines. Figure 6 displays constant volume fractions for 1, 2, 4, and 8 columns. The REV composed of 4 rows and 8 columns seems to be the most suitable for this structure as it will be closest to the value imposed in the topological optimization code. The final image will correspond to the dimensions (50×50).

4.2 Study of the dissimilarity between regular and irregular meshes













A first visual observation can be made regarding the facies of regular and irregular meshes (Tab. 3): the smaller the element size, the greater the number of internal branches in the structure. However, it can be noted that for an element size of 0.08 mm, the facies of the regular structure appears identical to that obtained for 0.1 mm and the number of internal branches decreases for the irregular one.

The volume fractions have, however, significantly degraded compared to the values entered by the user in the topological optimization code. This degradation is due to the manual cutting of images. The compliance rate has also been affected, not exceeding 80%. Nevertheless, given the direct correlation between compliance rate and volume fraction (Eqs. (12) and (14)), the volume fractions obtained by image processing on the final regular and irregular structures appear consistent with reality.

Table 2. REV size and facies obtained.

Image Facies					
Final size of image	(200 x 400)	(200 x 200)	(200 x 100)	(200 x 50)	(200 x 25)
REV size	(1 x 1)	(1 x 2)	(1 x 4)	(1 x 8)	(1 x 16)
Number of elements per REV	1	2	4	8	16
Image facies					
Final size of image	(100 x 400)	(100 x 200)	(100 x 100)	(100 x 50)	(100 x 25)
REV size	(2 x 1)	(2 x 2)	(2 x 4)	(2 x 8)	(2 x 16)
Number of elements per REV	2	4	8	16	32
Image facies					
Final size of image	(50 x 400)	(50 x 200)	(50 x 100)	(50 x 50)	(50 x 25)
REV size	(4 x 1)	(4 x 2)	(4 x 4)	(4 x 8)	(4 x 16)
Number of elements per REV	4	8	16	32	64
Image facies					
Final size of image	(25 x 400)	(25 x 200)	(25 x 100)	(25 x 50)	(25 x 25)
REV size	(8 x 1)	(8 x 2)	(8 x 4)	(8 x 8)	(8 x 16)
Number of elements per REV	8	16	32	64	128

Table 3. Facies, dissimilarity ratio vs element size.

Element size (mm)		Regular image	Irregular image		Soustraction
0.08	Faciès			Facies	
	$f_{v,th}$	0.5	0.5	$\Delta f_{v,th}$	0
	$f_{v,image}$	0.397	0.388	$\Delta f_{v,image}$	0.120
	τ_c	0.794	0.776	τ_d	0.240
0.1	Faciès			Facies	
	$f_{v,th}$	0.5	0.5	$\Delta f_{v,th}$	0
	$f_{v,image}$	0.396	0.395	$\Delta f_{v,image}$	0.141
	τ_c	0.792	0.790	τ_d	0.281
0.2	Faciès			Facies	
	$f_{v,th}$	0.5	0.5	$\Delta f_{v,th}$	0
	$f_{v,image}$	0.394	0.391	$\Delta f_{v,image}$	0.181
	τ_c	0.787	0.782	τ_d	0.362
0.25	Faciès			Facies	
	$f_{v,th}$	0.5	0.5	$\Delta f_{v,th}$	0
	$f_{v,image}$	0.392	0.394	$\Delta f_{v,image}$	0.147
	τ_c	0.784	0.788	τ_d	0.294

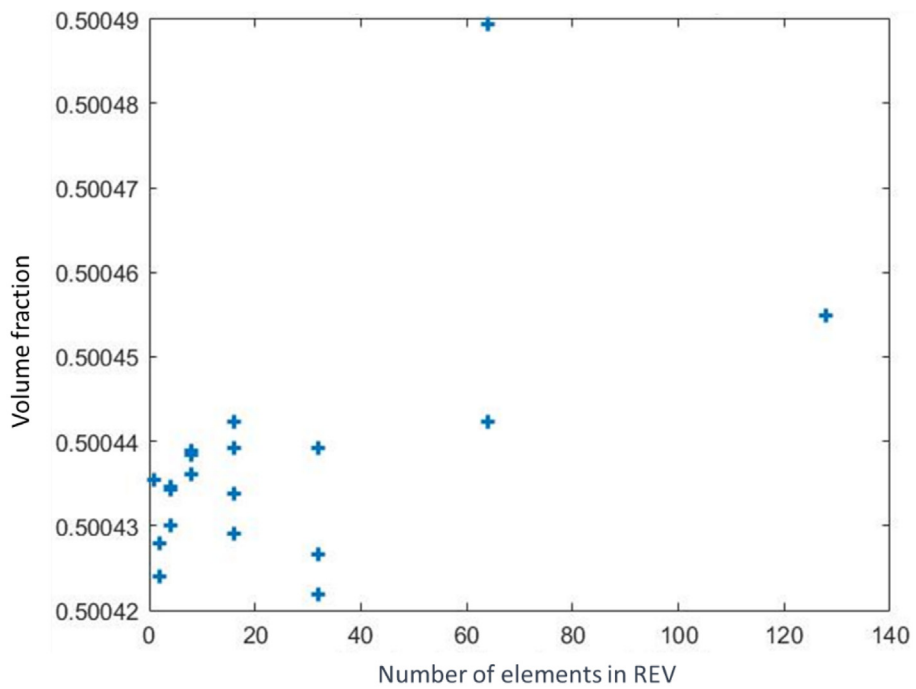


Fig. 4. Volume fraction vs number of elements in the REV.

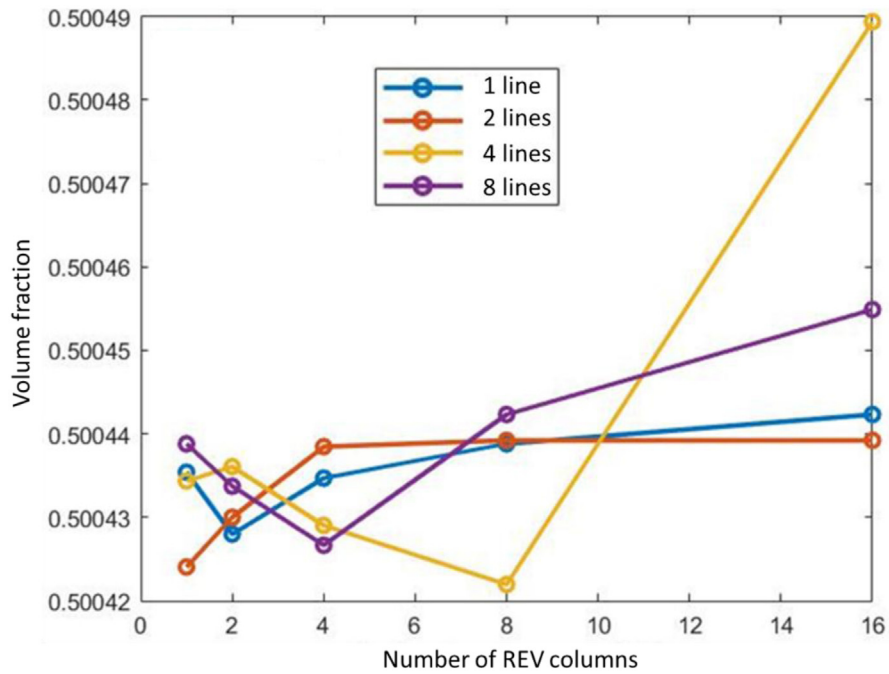


Fig. 5. Volume fraction vs number of columns in the REV.

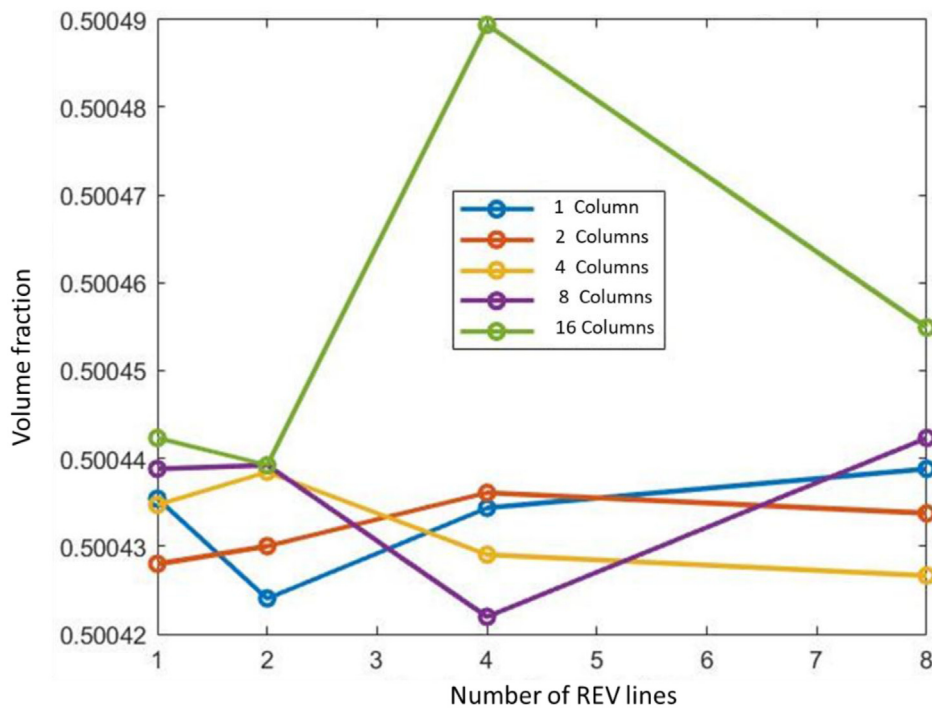


Fig. 6. Volume fraction vs number of lines in the REV.

For the image subtraction, white areas correspond to common material between regular and irregular meshes. The shaded areas correspond to excess material in one structure over the other. As the subtraction is absolute, it is not possible to determine which structure the excess comes from. Note that for visual purposes, each pixel has been subtracted by 255 to obtain a lighter image (black on white instead of white on black). However, this

subtraction is not performed for the calculation of the dissimilarity rate.

The dissimilarity rate tends to decrease with the element size, except for 0.2 mm where it is highest. This can be observed in the facies with numerous almost black branches. The dissimilarity rate is minimal for 0.08 mm, with a 24% difference between the two regular and irregular images. Further research could be conducted to reduce the

element size to determine if there is convergence in the dissimilarity rate.

5 Conclusion

Although the current results do not allow us to determine whether there is a link between the facies of the structure after topological optimization and its mechanical properties, they do highlight the potential applications that image processing could have on mechanical topological optimization problems.

It would be useful to define a way of finding the compliance using the image processing method, which would allow us to determine if a link exists between the structure's features and its mechanical properties. Since the application of the Representative Elementary Volume (REV) and image reduction did not have a significant influence on the volume fraction, if this result could be repeated for compliance, it would show that for a given mechanical problem, the result of the topology optimization would be independent of the structure's dimensions. Coupling this method with artificial intelligence would allow for a drastic reduction in the calculation times of the algorithm.

To improve the accuracy of the dissimilarity ratio, an image should be directly created from the unstructured mesh to avoid manually cutting the images. Increasing the conformity ratio could also have an impact on the dissimilarity ratio.

Based on the two features of the topology optimization, a manufacturability index could be characterized to determine which of the two structures is the most manufacturable.

6 Perspectives

It would be useful to define a way of calculating or finding compliance using image processing to determine whether there is a link between the mechanical properties of a structure and its facies. Since the application of a REV, and thus the reduction of an image, does not have a significant influence on the volume fraction of the structure, if this result were repeated for compliance, it would show that, for a given mechanical problem, the result of the topological optimization would be independent of the structure's dimensions. Coupling this method with artificial intelligence, which is currently being developed for the topological optimization code, would drastically reduce the calculation times of the algorithm.

To improve the accuracy of the dissimilarity rate, it would be wise to create an image directly from the

irregularly meshed structure to eliminate the need to cut out the images manually. Increasing the compliance rate could have a direct impact on the dissimilarity rate.

In view of the facies resulting from the topological optimization of both regularly and irregularly meshed structures, a manufacturability index could be characterized to determine which structure is more manufacturable.

References

1. O. Sigmund, A 99 line topology optimization code written in Matlab, *Struct. Multidisc. Optim.* **21**, 120–127 (2001) <https://doi.org/10.1007/s001580050176>
2. O. Sigmund, J. Petersson, B. Torstenfelt, A. Klöppel, Numerical instabilities in topology optimization: a survey on procedures dealing with checkerboards, mesh-dependencies and local minima, *Struct. Optim.* **16**, 68–75 (1998)
3. C.-J. Thore, H. Alm Grundström, Penalty regulation of overhang in topology optimization for additive manufacturing, *Struct. Multidisc. Optim.* **60**, 59–67 (2019)
4. ELIOT, Site official, Accès le 26 mars 2020. <https://www.openhub.net/p/eliot>
5. GMSH, Site official, Accès le 20 mars 2020. <https://gmsh.info/>
6. FreeCAD, Site official, Accès le 26 mars 2020. <https://www.freecadweb.org/?lang=fr>
7. Université Technologique de Compiègne, « Les fiches-notions de l'UTC sur la méthode des éléments finis. » [En ligne]. <http://www.utc.fr/~mecagom4/MECAWEB/accueil.html> (Accès le 4 Juin 2020)
8. T.C. Chu, W.F. Ranson, M.A. Sutton, Applications of digital-image-correlation to experimental mechanics, *Exp. Mech.* **25**, 232–244 (1985)
9. C. Bellis, M. Trabelsi, F. Frey, Identification de propriétés matérielles par traitement d'images de mesures de champs. In : CFM 2017-23ème Congrès Français de Mécanique. AFM, Maison de la Mécanique, 39/41 rue Louis Blanc-92400 Courbevoie. (2017)
10. E. Fagerholt, T. Børvik, O.S. Hopperstad, Measuring discontinuous displacement fields in cracked specimens using digital correlation with mesh adaptation and crack-path optimization, 23ème Congrès Français de Mécanique Opt Lasers Eng. **51**, 299–310 (2017)
11. RIVOLLIER, Séverine, DEBAYLE, Johan, et PINOLI, Jean-Charles. Analyse morphométrique d'images à tons de gris par diagrammes de forme. In : RFIA 2012 (Reconnaissance des Formes et Intelligence Artificielle) p. 978-2-9539515-2-3. (2012)
12. I. Sosnovik, I. Oseledets, Neural networks for topology optimization, *Russ. J. Numer. Anal. Math. Modell.* **34**, 215–223 (2019)
13. A. Ardeshir, Goshtasby, Similarity and Dissimilarity measures. *Image registration: Principles, tools and methods.* 7–66. (2012)

Cite this article as: Zoubir Atmani, Alexis Iung, Jean-Pierre Radoux, Nadhir Lebaal, Integration of digital imagery for topology optimization, *Int. J. Simul. Multidisci. Des. Optim.* **14**, 4 (2023)